Continuous tuning of spin-orbit coupled superconductivity in $NbSe_2$

Jia-Yi Ji,[1] Yi Hu,[1] Ting Bao,[1] Yong Xu,[1,2,3] Miaoling Huang,[4] Jianhao Chen,[4,5] Qi-Kun Xue,[1,3,4,6,*] and Ding Zhang[1,2,3,4,†]

[1]*State Key Laboratory of Low Dimensional Quantum Physics and Department of Physics, Tsinghua University, Beijing 100084, China*
[2]*RIKEN Center for Emergent Matter Science (CEMS), Wako, Saitama 351-0198, Japan*
[3]*Frontier Science Center for Quantum Information, Beijing 100084, China*
[4]*Beijing Academy of Quantum Information Sciences, Beijing 100193, China*
[5]*International Center for Quantum Materials, School of Physics, Peking University, Beijing 100091, China*
[6]*Southern University of Science and Technology, Shenzhen 518055, China*

(Received 18 March 2024; revised 17 August 2024; accepted 2 September 2024; published 11 September 2024)

$NbSe_2$ is expected to host a rich variety of quantum phenomena such as Ising superconductivity and the orbital Fulde-Ferrell-Larkin-Ovchinnikov (FFLO) state. So far, these intriguing states have been accessed only in discrete samples with a fixed set of parameters regarding the spin-orbit coupling strength, lattice symmetry, and dimensionality. Here, we invoke a lithium ion backgate to continuously tune those parameters and reveal a systematic evolution of superconductivity in both ultrathin and bulklike $NbSe_2$ samples. The ultrathin $NbSe_2$ after lithium intercalation possesses a further enhanced upper critical magnetic field over the Pauli limit, confirming the doping dependence of Ising superconductivity. Moreover, we successfully tune the bulklike $NbSe_2$ to a two-dimensional Ising superconductor at high doping. Additionally, at intermediate doping, we observe behaviors akin to the emergent orbital FFLO state.

DOI: 10.1103/PhysRevB.110.104509

I. INTRODUCTION

Cooper pairs with Ising-like spin orientations occur in two-dimensional (2D) spin-orbit coupled (SOC) superconductors [1]. This so-called Ising superconductivity was discovered in ultrathin superconductors with broken inversion symmetry [2–6] but was soon extended to centrosymmetric films with degenerate bands at high-symmetry points of the momentum space [7,8]. Among the Ising superconductors, ultrathin 2*H*-$NbSe_2$ [4] has been investigated extensively. A monolayer of $NbSe_2$ serves as a model system. Inversion symmetry breaking gives rise to opposite spin splitting of the hole bands at the K and K' points. Cooper pairing across these bands with spins locked to the out-of-plane direction are resilient to a magnetizing field transverse to the spin direction. This mechanism accounts for a largely enhanced in-plane upper critical field ($B_{c2}^{\parallel}$), more than six times the Pauli limit (B_p), in monolayer $NbSe_2$ [4]. Ultrathin $NbSe_2$ also distinguishes itself from conventional superconducting films by showing a gradual evolution of its superconducting gap with the applied in-plane magnetic field [9]. This behavior sharply differs from a sudden gap closing at a critical in-plane field observed in aluminum [10] and beryllium films [11]. Of late, the unusual gap-closing behavior and the twofold in-plane gap anisotropy [12–14] in few-layer $NbSe_2$, revealed by tunneling and magnetotransport experiments, hint at an additional exotic pairing component.

Apart from the studies in the 2D limit, there is a recent revival of interest in thicker forms of $NbSe_2$. By electrochemically intercalating large organic ions, bulk $NbSe_2$ was rendered to be an Ising superconductor with a strongly enhanced ratio of $B_{c2}^{\parallel}/B_p$ [15]. Similar enhancement was also achieved by growing misfit compounds such as $(LaSe)_{1.14}$-$NbSe_2$ [16]. These breakthroughs facilitate further investigations of the predicted enigmatic properties [1] because they allow for bulk sensitive techniques on Ising superconductors. Another major achievement was from $NbSe_2$ with a thickness ∼20 nm [17]. There, a meticulous two-axis rotation experiment unveiled sixfold in-plane anisotropy, lending strong support to the orbital Fulde-Ferrell-Larkin-Ovchinnikov (FFLO) state that was theoretically proposed recently [18]. Indication of this orbital FFLO state was also reported in lithium intercalated MoS_2 bilayers [19].

The above achievements were from samples with discrete thicknesses and at fixed densities. Exploration of the density dependence of Ising superconductivity, in terms of $B_{c2}^{\parallel}/B_p$, remains lacking. Theoretically, spin splitting in an Ising superconductor should become stronger as the Fermi level shifts closer to the band tops at the K and K' points. Reducing the hole concentrations would further enhance Ising pairing, giving rise to a larger $B_{c2}^{\parallel}/B_p$. Additionally, bulklike $NbSe_2$ (thickness ≳20 nm) is a superconductor in the clean limit. How this clean superconductor evolves to be an Ising superconductor after intercalation [15] remains to be elucidated. These investigations require effective tuning of the carrier density of $NbSe_2$. However, $NbSe_2$ is well in the metallic regime, and its carrier density is as high as 10^{15} cm^{-2} per layer. Addressing the doping dependence of superconductivity in $NbSe_2$ thus demands gating techniques beyond the standard electrostatic field effect. To this purpose, ionic liquid gating was employed to tune a bilayer $NbSe_2$ with its carrier density

*Contact author: qkxue@mail.tsinghua.edu.cn
†Contact author: dingzhang@mail.tsinghua.edu.cn

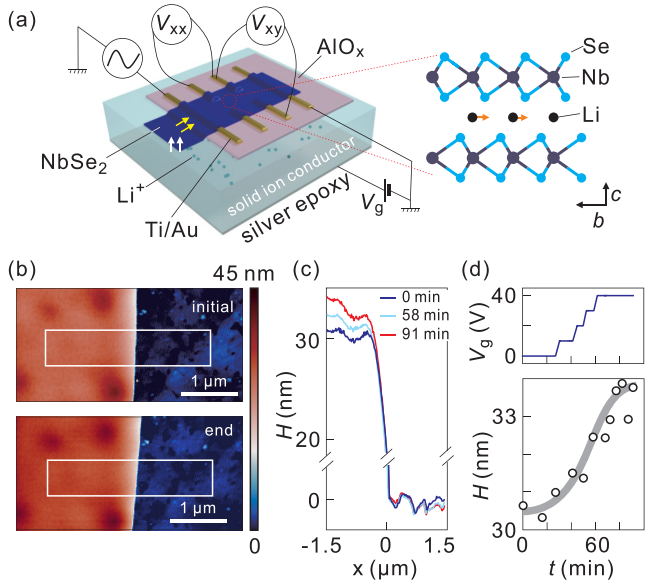

FIG. 1. (a) Schematic drawing of a $NbSe_2$ flake under lateral lithium intercalation. White arrows indicate the direct intercalation of lithium ions from the solid ion conductor. Yellow arrows indicate the lateral diffusion of lithium ions to the $NbSe_2$ flake on top of the AlO_x blocking layer. Right panel provides a stick-ball model of $NbSe_2$ with lithium ions in the interlamellar gap. (b) Topographic images of $NbSe_2$ before and after the lateral lithium intercalation. The image is taken by using an *in situ* atomic force microscopy (AFM; contact mode, scanning frequency: 1 Hz) in an Argon-filled glove box. The scanned region is located on the AlO_x buffer. White rectangles indicate the areas for estimating the height of the flake. (c) Representative height profiles taken at different gated stages. (d) AFM determined sample height as a function of gating time. Upper panel shows the corresponding backgate voltage.

modulated by ∼10% [20]. Recently, ion backgating has been demonstrated to tune superconductivity of $NbSe_2$ in a broader density range [21,22], but the corresponding critical magnetic field remains unexplored.

Here, we study the evolution of B_{c2} in $NbSe_2$ over a wide range of carrier density by ion backgating. In few-layer $NbSe_2$, we demonstrate that lithium intercalation results in a further enhancement of $B_{c2}^{\parallel}/B_p$. In bulklike $NbSe_2$, we unveil a gradual transition of its magnetic field response from an anisotropic three-dimensional system to a purely 2D superconductor. The enhanced $B_{c2}^{\parallel}/B_p$ after extensive lithium intercalation becomes comparable with that reported for a trilayer $NbSe_2$. Also, the bulklike superconductor at intermediate doping remains in the clean limit and exhibits features akin to that of an orbital FFLO state. These observations indicate that lithium intercalation can dramatically enhance the 2D character of $NbSe_2$, consistent with the expectation for Ising superconductors.

II. EXPERIMENTAL RESULTS

A. Sample fabrication and technical details

We employ our recently developed lateral intercalation scheme for tuning $NbSe_2$ [22]. Figure 1(a) is a schematic drawing of our device. The substrate is a solid ion conductor (SIC) [23] with the chemical formula: Li_2O-Al_2O_3-SiO_2-P_2O_5-TiO_2-GeO_2. We patterned a square of AlO_x [$100\times100\,\mu m^2$, pink in Fig. 1(a)] with a thickness of 15 nm by e-beam lithography (EBL) and atomic layer deposition. Our previous experiment demonstrated that the AlO_x layer can block the direct penetration of lithium [22]. After growing the blocking layer, we patterned the electrodes (Ti/Au, 10 nm/30 nm) by EBL and loaded the substrate into a glovebox with Ar atmosphere (H_2O < 0.1 ppm, O_2 < 0.1 ppm). In the glovebox, we mechanically exfoliated the single crystal of $NbSe_2$. We then dry transferred [24] the $NbSe_2$ flake [dark blue in Fig. 1(a)] onto the targeted area of the substrate such that it covered both the AlO_x region and the exposed surface of SIC.

The sample thickness was typically determined by atomic force microscopy (AFM) immediately after the sample fabrication. Afterwards, we carried out lithium intercalation and magnetotransport experiments. The gating process was carried out at room temperature (300 K). This process can be reversed by applying negative voltages. It was terminated at low temperatures (<200 K) for transport studies. Electrical measurements were performed with the standard lock-in technique. The typical excitation current was chosen to be 1 μA (13.333 Hz). The carrier density was determined by measuring the Hall effect of the sample at 50 K. The angular-dependent study was carried out by rotating the sample *in situ* via a home-built sample holder with a piezorotator.

B. Topographic study

Applying a certain positive backgate voltage can drive lithium ions first into the region of $NbSe_2$ in direct contact to SIC, as indicated by white arrows in Fig. 1(a). The intercalated lithium ions then migrate via the interlamellar gap of $NbSe_2$ and permeate to the complete flake (yellow arrows). In Figs. 1(b)–1(d), we carry out an *in situ* topographic study of the sample during the intercalation. Our previous AFM study at ambient condition [22] indicated that the intercalated lithium may react with water and forms hydrated compounds inside the interlamellar gap. To avoid this chemical reaction, we now carry out the AFM study in an argon-filled glovebox.

Figure 1(b) shows the typical AFM images taken before and after the lithium intercalation. The slightly darker color in the left part of the image after intercalation indicates the increase of sample height. We estimate the height of $NbSe_2$ by averaging over the line profiles in a certain region close to the step edge [white rectangle]. Figure 1(c) shows the averaged results at different gating stages. We summarize the sample height as a function of gating in Fig. 1(d). Clearly, the height of the sample increases from the initial value of ∼30.5–33.5 nm at the end. It corresponds to an expansion ratio of ∼10% in the *c* axis, in agreement with the previous study on chemically intercalated $NbSe_2$ [25]. We note that the AFM study is taken in the region located on the AlO_x blocking layer. The increase in height confirms the successful lateral migration of the intercalated lithium ions.

C. Continuous tuning of the superconducting transition

In Figs. 2(a) and 2(b), we show representative curves of resistance at low temperatures for few-layer (sample S1,

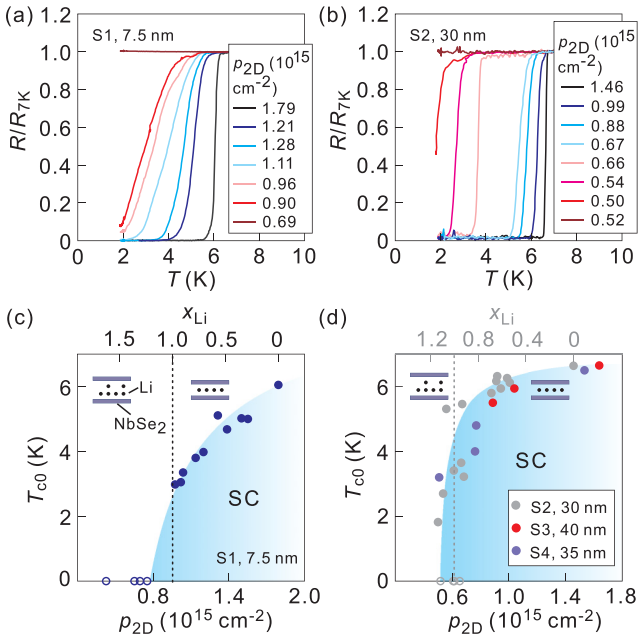

FIG. 2. (a) and (b) Temperature-dependent resistances of two lithium intercalated $NbSe_2$ samples (S1 and S2) with distinctly different thicknesses. The resistance is normalized by the value at 7 K. Hole densities per Se-Nb-Se layer are obtained from the Hall effect at 50 K for each state. (c) and (d) Superconducting transition temperature T_{c0} as a function of carrier density per layer for a few-layer $NbSe_2$ (S1) and three bulklike samples (S2–S4). Empty circles represent the states in which superconducting transition is not observed down to the lowest temperature (1.9 K) of our instrument. Insets illustrate the distribution of lithium ions in the interlamellar gap. Top abscissa reflect the estimated lithium content for samples S1 and S2, respectively.

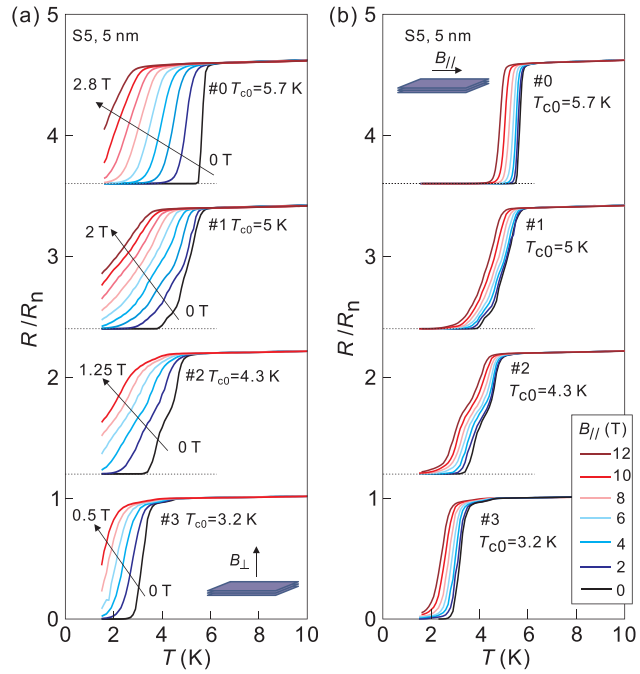

FIG. 3. (a) and (b) Temperature-dependent normalized resistances of sample S5 (5 nm thick) under different lithium intercalation and at a series of out-of-plane/in-plane magnetic fields. #0 denotes the pristine state. Curves for different states are vertically offset for clarity. Dotted lines represent zero resistance for the different states. The out-of-plane magnetic fields applied for states #0/#1/#2/#3 are from 0 to 2.8/2/1.25/0.5 T with intervals of 0.35/0.25/0.25/0.1 T.

7.5 nm, 12 layers) and bulklike (sample S2, 30 nm, 48 layers) $NbSe_2$, respectively. With consecutive gating, superconducting transitions of the two samples gradually move to lower temperatures. The suppression of superconductivity stems from a reduced total carrier density in $NbSe_2$: Electron doping of lithium counteracts the predominant charge carriers of holes. This density tuning is confirmed by low-temperature Hall effect measurements at 50 K for each gate state (above the temperature for charge density wave of bulk $NbSe_2$ $T_{CDW} = 32$ K).

Figures 2(c) and 2(d) summarize the superconducting transition temperature T_{c0} of the gated states as a function of the hole carrier density per Se-Nb-Se layer p_{2D}. Here, we determine T_{c0} as the temperature point where the resistance drops to half of the normal state value R_n at zero magnetic field. For sample S1(S2), we can tune p_{2D} from 1.8×10^{15} to 0.4×10^{15} cm^{-2} (1.5×10^{15} to 0.5×10^{15} cm^{-2}). It corresponds to a density tuning of 78% (66%), which is dramatic in a metallic system [21]. From the variation of p_{2D}, we estimate the lithium content [top abscissa in Figs. 2(c) and 2(d)] by using an effective charge transfer ratio of 0.86 [26] for each lithium ion [27]. The maximum lithium content reaches as high as 160% for sample S1 and 115% for sample S2. It indicates that a second layer of lithium ions starts to form within the interlamellar gap [schematically shown as inset to Figs. 2(c) and 2(d)].

D. B_{c2} in few-layer $NbSe_2$

After demonstrating the wide tunability, we study the evolution of B_{c2}. We realize gated states with different T_{c0} in a few-layer $NbSe_2$ (sample S5, 5 nm thick). To enhance the uniformity of lithium distribution, we carry out several cycles of lithiation and delithiation [19,28]. For each gated state of sample S5, we investigate its response to the in-plane and out-of-plane magnetic fields. Figure 3(a) shows that, in the perpendicular configuration, the required magnetic field for suppressing superconductivity becomes much smaller as T_{c0} decreases. By contrast, the superconducting state remains resilient to the in-plane magnetic field after lithium intercalation. Even for state #3 with a reduced T_{c0} of 3.2 K, applying the highest magnetic field of 12 T only increases the resistance slightly at 2 K.

The above behaviors can be quantified by extracting the temperature dependences of the upper critical fields $B_{c2}^{\perp}$ and $B_{c2}^{\parallel}$ (we use the midpoint criterion). In Figs. 4(a) and 4(b), we plot the extracted $B_{c2}^{\perp}$ and $B_{c2}^{\parallel}$ as a function of temperature. Figures 4(c) and 4(d) show the same datasets but with B_{c2} normalized by B_p. Here, we employ the conventional relation of $B_p = 1.86T_{c0}$ for the normalization. It assumes a standard gap-to-T_c ratio of 1.76 and a g-factor of 2. We note that, in reality, the conversion factor may differ from 1.86 and can vary with lithium doping. With this caveat in mind, $B_{c2}/(1.86T_{c0})$

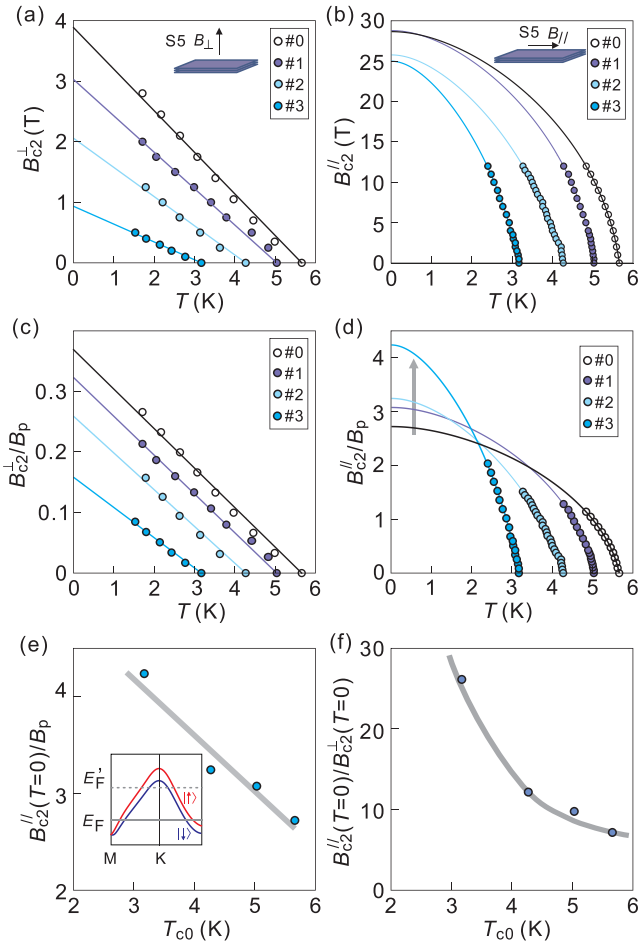

FIG. 4. (a) and (b) Temperature dependences of the out-of-plane/in-plane B_{c2} for states #0 to #3 of sample S5. (c) and (d) Temperature dependences of the out-of-plane/in-plane B_{c2} normalized by B_p for the same sample. Lines in (a) and (c) are from the linear fitting. Curves in (b) and (d) are theoretical fits by using the Werthamer-Helfand-Hohenberg (WHH) formula. (e) Extrapolated zero-temperature in-plane upper critical field $B_{c2}^{\parallel}(T=0)$ normalized by B_p as a function of T_{c0}. Inset illustrates the spin-split bands of $NbSe_2$ around the K point. Horizontal lines marked by E_F and E_F' schematically indicate the upward shift of the Fermi level. (f) Anisotropic factor $B_{c2}^{\parallel}/B_{c2}^{\perp}$ as a function of T_{c0}.

helps compare the results obtained at different T_{c0}'s. To extract B_{c2} $(T=0)$, we employ the Werthamer-Helfand-Hohenberg (WHH) formula [29] to fit the in-plane data and use a linear fitting for the out-of-plane data. The same trend of $B_{c2}^{\parallel}$ $(T=0)$ as a function of T_{c0} can be obtained by fitting with the 2D Ginzburg-Landau (GL) formula, as shown in the Appendix.

Figure 4(a) indicates that $B_{c2}^{\perp}$ $(T=0)$ is suppressed by nearly a factor of four from state #0 to state #3. By contrast, $B_{c2}^{\parallel}$ $(T=0)$ slightly decreases from ~30 to 25 T as T_{c0} drops from 5.7 to 3.2 K [Fig. 4(b)]. It reflects not only a larger anisotropy ratio with lithium intercalation but also a relative enhancement of $B_{c2}^{\parallel}$ with respect to the reduced T_{c0}. These effects are better captured by Figs. 4(d)–4(e). They indicate a continuous enhancement of $B_{c2}^{\parallel}$ $(T=0)$ over B_p. This behavior is consistent with the expectation of Ising superconductivity. Namely, the uplift of the Fermi level by lithium intercalation enhances the effective Zeeman spin splitting around the K and K' points [illustrated by the inset of Fig. 4(e)]. The resultant Cooper pairs become more robust against an in-plane magnetic field.

Figure. 4(f) shows that $B_{c2}^{\parallel}$ $(T=0)/B_{c2}^{\perp}$ $(T=0)$ increases by a factor of four with decreasing T_{c0}. For a further analysis, we employ

$$B_{c2}^{\perp}(T=0) = \frac{\Phi_0}{2\pi\xi^2}, \tag{1}$$

$$B_{c2}^{\parallel}(T=0) = \frac{\sqrt{12}\Phi_0}{2\pi\xi d_{sc}}, \tag{2}$$

where $\Phi_0 = h/2e$ is the flux quantum, ξ is the in-plane superconducting coherent length, and d_{sc} is the superconducting thickness. From state #0 to state #3, the estimated d_{sc} decreases from 4.3 to 2.4 nm. Such a 50% variation seems unlikely to stem solely from the lattice expansion induced by lithium intercalation, which is only ~10% (as shown in Fig. 1). Instead, we argue that the enhanced anisotropy with lithium intercalation is largely due to the shrinking Se-derived band around the Γ point as the Fermi level moves up. This band is more dispersive in the c axis; thus, the reduction of its contribution strongly promotes the 2D character of $NbSe_2$ [30,31]. Similar suppression of the Se-derived band has been recently observed in the misfit compound of $(LaSe)_{1.14}$-$NbSe_2$ as a result of electron doping to the $NbSe_2$ layer [16].

E. B_{c2} in bulklike $NbSe_2$

We now study B_{c2} in three bulklike $NbSe_2$ samples under lithium intercalation: S3 (40 nm), S4 (35 nm), and S6 (30 nm). Figures 5(a) and 5(b) collect the resistance data under a series of out-of-plane and in-plane magnetic fields. Figures 6(a) and 6(b) plot the extracted $B_{c2}^{\perp}(T)$ and $B_{c2}^{\parallel}(T)$. In Figs. 6(c) and 6(d), we normalize $B_{c2}^{\perp}$ and $B_{c2}^{\parallel}$ by B_p (We again use the standard conversion: $B_p = 1.86T_{c0}$). Figures 6(a) and 6(c) show that $B_{c2}^{\perp}(T)$ always follows the linear behavior, and $B_{c2}^{\perp}(0)$ gets prominently suppressed with lithium intercalation. This evolution is like that observed in few-layer $NbSe_2$. Figures 6(b) and 6(d) show that $B_{c2}^{\parallel}(T)$ gradually transitions from a linear behavior for the pristine state to a parabolic behavior after lithium intercalation. For the state with $x_{Li} = 1.2$, $B_{c2}^{\parallel}(T)$ closely follows the 2D GL formula (dotted curve). It suggests that such a bulklike sample becomes analogous to a purely 2D superconductor.

Indeed, by using Eqs. (1) and (2), we estimate that d_{sc} is 3.7 nm for $x_{Li} = 1.2$, much smaller than the sample thickness (35 nm). Figure 6(e) further summarizes the extracted $B_{c2}^{\parallel}$ $(T=0)$ normalized by B_p. At high doping level with $x_{Li} = 1.2$, the extrapolated $B_{c2}^{\parallel}$ $(T=0)$ reaches about three times B_p. Such a large $B_{c2}^{\parallel}$ $(T=0)/B_p$ ratio is comparable with that observed in a trilayer $NbSe_2$ [9]. Meanwhile, the anisotropy ratio $B_{c2}^{\parallel}$ $(T=0)/B_{c2}^{\perp}$ $(T=0)$ is enhanced by a factor of five after lithium intercalation [Fig. 6(f)].

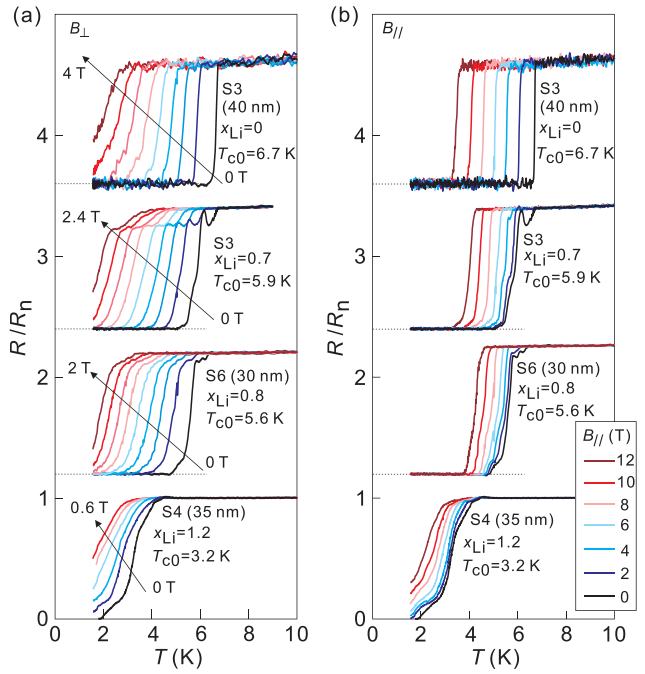

FIG. 5. (a) and (b) Temperature-dependent normalized resistances of samples S3 (40 nm), S4 (35 nm), and S6 (30 nm) with different contents of lithium ions and at a series of out-of-plane/in-plane magnetic fields. Curves for different states are vertically offset for clarity. Dotted lines represent zero resistance for the different states. The out-of-plane magnetic fields applied for state $x_{Li} = 0, 0.7, 0.8, 1.2$ are from 0 to 4/2.4/2/0.6 T with intervals of 0.5/0.3/0.25/0.12 T.

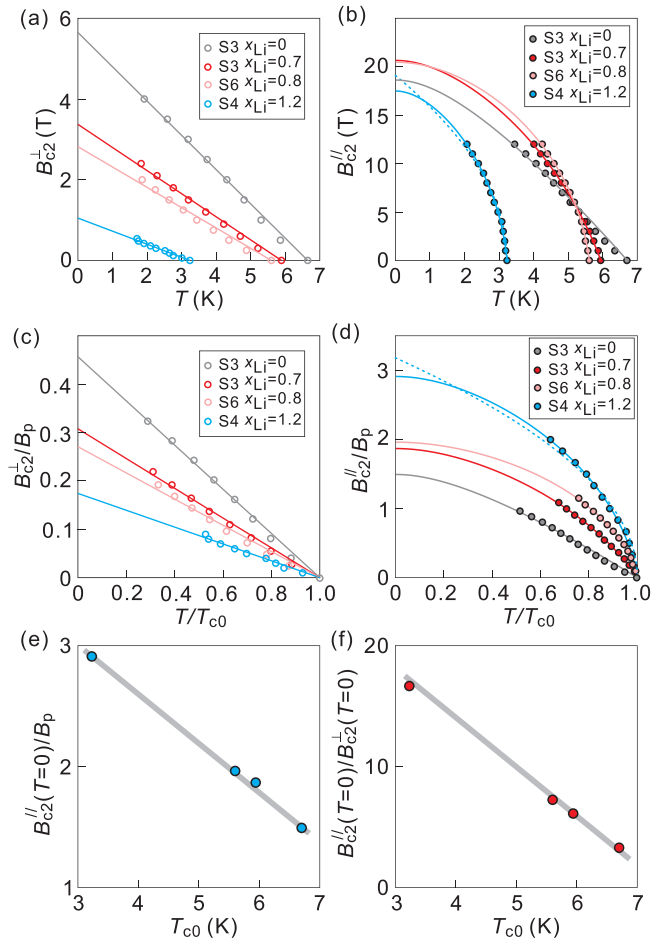

FIG. 6. (a) and (b) Temperature dependences of the out-of-plane/in-plane B_{c2} for state with $x_{Li} = 0, 0.7, 0.8, 1.2$. (c) and (d) Temperature dependences of the out-of-plane/in-plane B_{c2} normalized by the corresponding B_p. Lines in (a) and (c) are from the linear fitting. Solid/dashed curves in (b) and (d) are theoretical fits by using the Werthamer-Helfand-Hohenberg (WHH)/two-dimensional (2D) Ginzburg-Landau (GL) formula. (e) Extrapolated $B_{c2}^{\parallel}(T = 0)$ normalized by B_p as a function of T_{c0}. (f) Anisotropic factor $B_{c2}^{\parallel}/B_{c2}^{\perp}$ as a function of T_{c0}.

F. Angular dependence of B_{c2} in bulklike $NbSe_2$

Recent experiments [17] have indicated that the clean superconductor of $NbSe_2$ with a moderate thickness may host the enigmatic orbital FFLO state under a certain in-plane magnetic field. We point out that our bulklike superconducting $NbSe_2$, even after lithium intercalation, seems to be in the clean limit too. The estimated superconducting coherence lengths for sample S3 with $x_{Li} = 0$ and 0.7, using Eq. (1) and the data in Fig. 6(a), are ∼8 and 10 nm. These values are much smaller than the corresponding mean free paths of the same states: 29 and 26 nm (see Appendix B for the estimation). One key feature of the reported FFLO state comes from the angular dependence of B_{c2}: It hosts a sharper cusp around the in-plane situation than that based on the 2D Tinkham model [17,32]. In the following, we study the angular dependence of B_{c2} in our bulklike $NbSe_2$ samples.

Figures 7(a) and 7(b) show the angular dependence of B_{c2} of sample S3 with $x_{Li} = 0$. The data points around $\theta = 0^\circ$ constitute a cusp that is sharper than that from a 2D Tinkham model [Fig. 7(b), solid curve]. The same behavior can be seen for sample S6 [Figs. 9(a) and 9(b)]. We comment that the deviation ∼0° is not as pronounced as that reported before [17]. This is possibly due to the stronger interlayer coupling in our relatively thicker samples.

Interestingly, the cusp becomes more pronounced after lithium intercalation and deviates more strongly from the 2D Tinkham model [Figs. 7(c), 7(d), 9(c), and 9(d)]. We argue that this enhancement is not a result of wrinkles or inhomogeneities caused by lithium intercalation because (1) we employ a lateral intercalation scheme such that lithium distribution is quite uniform, as demonstrated in our previous report [22]; (2) the enhanced cusp ∼0° is observed only when $\xi < l$ is satisfied. By further increasing the lithium concentration, l drops such that the sample returns to the dirty limit. There, no enhanced cusp can be observed for $B_{c2}(\theta)$, although lithium intercalation presumably increases inhomogeneity. Such a recovery to the standard 2D Tinkham model can be seen for sample S4 with $x_{Li} = 1.2$ [Figs. 7(e) and 7(f)].

Instead, the enhanced sharp feature of B_{c2} at ∼0°, for the intermediately doped samples, seems consistent with the feature reported for the orbital FFLO state. As demonstrated in Fig. 6, lithium intercalation promotes Ising superconductivity and weakens interlayer coupling in our bulklike samples. In addition, the expanded interlayer spacing after lithium intercalation can give rise to a larger center-of-mass momentum

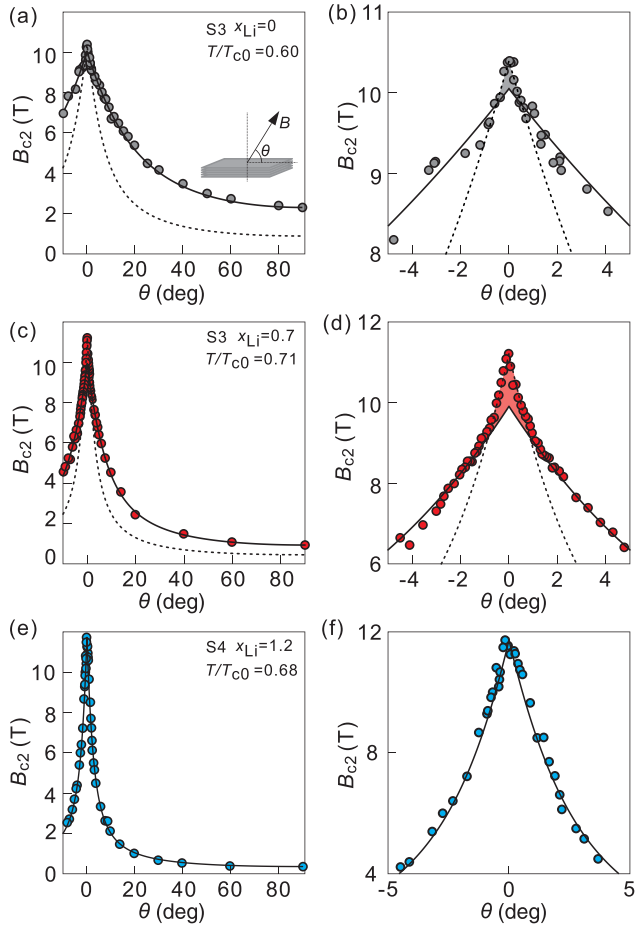

FIG. 7. (a) and (b) Angular dependences of B_{c2} of sample S3 in the pristine state. Solid/dashed curves are two-dimensional (2D) Tinkham fitting to the data points with $|\theta| > 1.5^\circ/|\theta| < 0.5^\circ$. Inset in (a) indicates the orientation of the magnetic field relative to the sample plane. (c) and (d) Angular dependences of B_{c2} for sample S3 with $x_{Li} = 0.7$. Solid/dashed curves are 2D Tinkham fitting to the data points with $|\theta| > 1.5^\circ/|\theta| < 0.5^\circ$. (e) and (f) Angular dependence of B_{c2} for sample S4 with $x_{Li} = 1.2$. Solid curve is the fitting by using the 2D Tinkham formula.

shift of the Cooper pairs under the applied in-plane magnetic field. These effects can help stabilize the orbital FFLO state.

III. DISCUSSION

The conversion from a bulk superconductor to a 2D Ising superconductor is remarkable. A similar dimensional reduction effect was recently realized by intercalating large organic molecules to bulk $NbSe_2$ [15]. There, the c-axis expansion was as large as 63%. In sharp contrast, lithium intercalation employed here only causes a limited expansion (Fig. 1). Here, we speculate on the unique role of the intercalated lithium. First, a positively charged layer of lithium ions can effectively screen the Coulomb interaction between different $NbSe_2$ layers, suppressing the interlayer interaction. Secondly, by slightly exceeding a 1:1 ratio between Li and Nb, a second layer of lithium ions starts to accumulate on top of the first layer inside the interlamellar gaps [insets of Figs. 2(c) and 2(d)]. This piling of lithium ions obviously breaks inversion symmetry. Although lithium ions in reality may distribute more randomly, the tendency of breaking inversion symmetry of the lattice still persists in local areas. It enhances the SOC effect and promotes Ising superconductivity.

In summary, we investigate the systematic evolution of B_{c2} in $NbSe_2$ by electric-field-controlled lithium intercalation. We obtain an enhanced $B_{c2}^{\parallel}/B_p$ in ultrathin $NbSe_2$ after intercalation, consistent with the expected behavior of Ising superconductivity. In bulklike $NbSe_2$, lithium intercalation can convert the system to a stack of 2D Ising superconductors at high doping. Also, moderate lithium doping seems to promote the features of the orbital FFLO state. Our results demonstrate the distinct role of lithium ions in tuning SOC superconductivity.

ACKNOWLEDGMENT

This paper is financially supported by the National Natural Science Foundation of China (Grants No. 12361141820, No. 12274249, and No. 52388201).

APPENDIX A: $B_{c2}^{\parallel}(T)$ FIT BY THE 2D GL FORMULA

In Fig. 8(a), we employ the 2D GL formula to fit the in-plane upper critical field for sample S5. Figure 8(b) summarizes the extrapolated $B_{c2}^{\parallel}$ $(T = 0)$ normalized by B_p. These results also show the continuous enhancement of $B_{c2}^{\parallel}$ $(T = 0)/B_p$.

APPENDIX B: EVALUATION OF THE MEAN FREE PATH

We carry out Hall effect measurements for our samples at different gated states at 50 K. The obtained Hall resistances as a function of magnetic field always show linear behaviors with positive slopes (up to the maximum field of 6 T that we applied). It suggests that the CDW temperature remains <50 K throughout the lithium intercalation. Otherwise, the Hall effect at 50 K may show a negative slope at certain dopings. We obtain the hole carrier density p from the slope of the Hall resistance and estimate the mean free path:

$$l = \frac{h/e^2}{R_s\sqrt{2\pi g_v p}}. \tag{B1}$$

Here, g_v represents the valley degeneracy (the spin degeneracy of two has been considered), and R_s is the sheet resistance. We

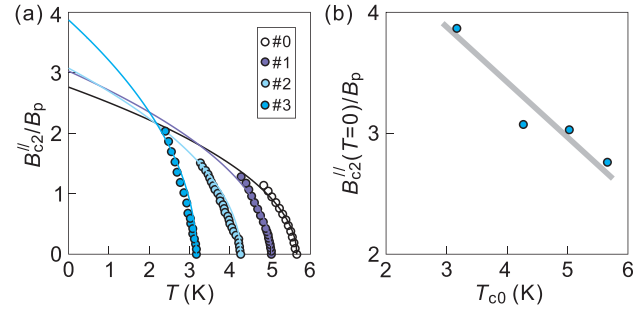

FIG. 8. (a) Temperature dependences of the in-plane B_{c2} normalized by B_p for sample S5 in states #0 to #3. Solid curves are fits by using the two-dimensional (2D) Ginzburg-Landau (GL) formula. (b) Extrapolated $B_{c2}^{\parallel}$ $(T = 0)$ normalized by B_p as a function of T_{c0}.

TABLE I. Evaluated mean free path and the corresponding superconducting coherence length for the bulklike $NbSe_2$ samples. We use the relation $\xi_p = 1.35\xi_{GL}(0)$ for obtaining the Pippard coherence length.

Sample	l (nm)	$\xi_{GL}(0)$ (nm)	ξ_p (nm)
S3, $x_{Li} = 0$	28.77	7.63	10.31
S3, $x_{Li} = 0.7$	25.79	9.88	13.34
S4, $x_{Li} = 1.2$	8.93	17.71	23.91
S6, $x_{Li} = 0.6$	22.56	9.84	13.29

use $g_v = 3$ for the three hole bands in $NbSe_2$. The electron band of $NbSe_2$, which is prominent in the Seebeck effect [33], is neglected here since the Hall effect shows dominating behavior of holes. The estimated values of l are given in Table I.

APPENDIX C: EXTENDED DATA ON BULKLIKE $NbSe_2$ WITH INTERMEDIATE LITHIUM INTERCALATION

Figure 9 shows the angular dependence of B_{c2} for sample S6. We compare the data obtained in the pristine state and that after lithium intercalation ($x_{Li} = 0.6$). Like sample S3 with $x_{Li} = 0.7$, the lithium intercalated state shows a pronounced cusp in the angular dependence of B_{c2} around in-plane direction [Figs. 9(c) and 9(d)], sharper than that expected from a standard 2D Tinkham model.

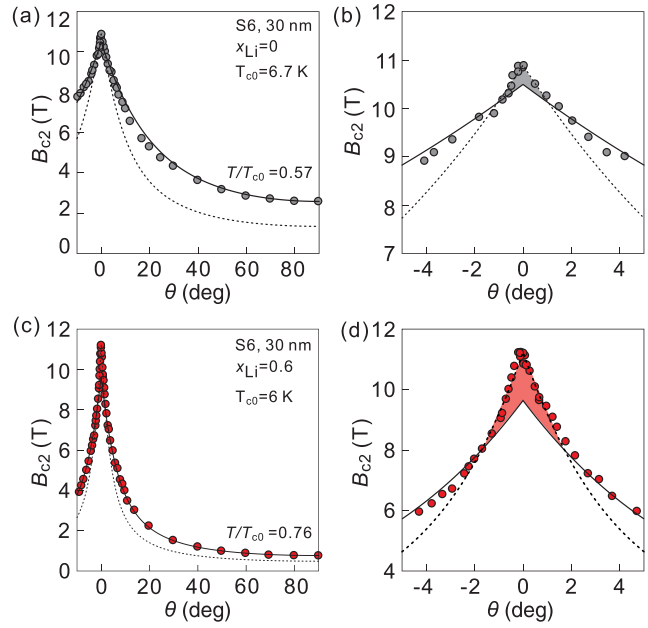

FIG. 9. (a) and (b) Angular dependence of B_{c2} for sample S6 in the pristine state. Solid/dashed curves are two-dimensional (2D) Tinkham fitting to the data points with $|\theta| > 1.5°/|\theta| < 1°$. (c) and (d) Angular dependence of B_{c2} for sample S6 with $x_{Li} = 0.6$. Solid/dashed curves are 2D Tinkham fitting to the data points with $|\theta| > 1.5°/|\theta| < 1°$.

[1] D. Zhang and J. Falson, Ising pairing in atomically thin superconductors, Nanotechnology **32**, 502003 (2021).

[2] J. Lu, O. Zheliuk, I. Leermakers, N. F. Yuan, U. Zeitler, K. T. Law, and J. Ye, Evidence for two-dimensional Ising superconductivity in gated MoS_2, Science **350**, 1353 (2015).

[3] Y. Saito, Y. Nakamura, M. S. Bahramy, Y. Kohama, J. Ye, Y. Kasahara, Y. Nakagawa, M. Onga, M. Tokunaga, T. Nojima *et al.*, Superconductivity protected by spin-valley locking in ion-gated MoS_2, Nat. Phys. **12**, 144 (2016).

[4] X. Xi, Z. Wang, W. Zhao, J.-H. Park, K. T. Law, H. Berger, L. Forró, J. Shan, and K. F. Mak, Ising pairing in superconducting $NbSe_2$ atomic layers, Nat. Phys. **12**, 139 (2016).

[5] S. C. de la Barrera, M. R. Sinko, D. P. Gopalan, N. Sivadas, K. L. Seyler, K. Watanabe, T. Taniguchi, A. W. Tsen, X. Xu, D. Xiao *et al.*, Tuning Ising superconductivity with layer and spin-orbit coupling in two-dimensional transition-metal dichalcogenides, Nat. Commun. **9**, 1427 (2018).

[6] J. Lu, O. Zheliuk, Q. Chen, I. Leermakers, N. E. Hussey, U. Zeitler, and J. Ye, Full superconducting dome of strong Ising protection in gated monolayer WS_2, Proc. Natl. Acad. Sci. USA **115**, 3551 (2018).

[7] J. Falson, Y. Xu, M. Liao, Y. Zang, K. Zhu, C. Wang, Z. Zhang, H. Liu, W. Duan, K. He *et al.*, Type-II Ising pairing in few-layer stanene, Science **367**, 1454 (2020).

[8] Y. Liu, Y. Xu, J. Sun, C. Liu, Y. Liu, C. Wang, Z. Zhang, K. Gu, Y. Tang, C. Ding *et al.*, Type-II Ising superconductivity and anomalous metallic state in macro-size ambient-stable ultrathin crystalline films, Nano Lett. **20**, 5728 (2020).

[9] E. Sohn, X. Xi, W.-Y. He, S. Jiang, Z. Wang, K. Kang, J.-H. Park, H. Berger, L. Forró, K. T. Law *et al.*, An unusual continuous paramagnetic-limited superconducting phase transition in 2D $NbSe_2$, Nat. Mater. **17**, 504 (2018).

[10] R. Meservey, P. Tedrow, and R. C. Bruno, Tunneling measurements on spin-paired superconductors with spin-orbit scattering, Phys. Rev. B **11**, 4224 (1975).

[11] P. W. Adams, P. Herron, and E. I. Meletis, First-order spin-paramagnetic transition and tricritical point in ultrathin Be films, Phys. Rev. B **58**, R2952(R) (1998).

[12] A. Hamill, B. Heischmidt, E. Sohn, D. Shaffer, K.-T. Tsai, X. Zhang, X. Xi, A. Suslov, H. Berger, L. Forró *et al.*, Two-fold symmetric superconductivity in few-layer $NbSe_2$, Nat. Phys. **17**, 949 (2021).

[13] C.-w. Cho, J. Lyu, L. An, T. Han, K. T. Lo, C. Y. Ng, J. Hu, Y. Gao, G. Li, M. Huang *et al.*, Nodal and nematic superconducting phases in $NbSe_2$ monolayers from competing superconducting channels, Phys. Rev. Lett. **129**, 087002 (2022).

[14] M. Kuzmanović, T. Dvir, D. LeBoeuf, S. Ilić, M. Haim, D. Möckli, S. Kramer, M. Khodas, M. Houzet, J. S. Meyer *et al.*, Tunneling spectroscopy of few-monolayer $NbSe_2$ in high magnetic fields: Triplet superconductivity and Ising protection, Phys. Rev. B **106**, 184514 (2022).

[15] H. Zhang, A. Rousuli, K. Zhang, L. Luo, C. Guo, X. Cong, Z. Lin, C. Bao, H. Zhang, S. Xu *et al.*, Tailored Ising superconductivity in intercalated bulk $NbSe_2$, Nat. Phys. **18**, 1425 (2022).

[16] T. Samuely, D. Wickramaratne, M. Gmitra, T. Jaouen, O. Šofranko, D. Volavka, M. Kuzmiak, J. Haniš, P. Szabó, C.

Monney *et al.*, Protection of Ising spin-orbit coupling in bulk misfit superconductors, Phys. Rev. B **108**, L220501 (2023).

[17] P. Wan, O. Zheliuk, N. F. Yuan, X. Peng, L. Zhang, M. Liang, U. Zeitler, S. Wiedmann, N. E. Hussey, T. T. Palstra *et al.*, Orbital Fulde-Ferrell-Larkin-Ovchinnikov state in an Ising superconductor, Nature (London) **619**, 46 (2023).

[18] C.-X. Liu, Unconventional superconductivity in bilayer transition metal dichalcogenides, Phys. Rev. Lett. **118**, 087001 (2017).

[19] D. Zhao, L. Debbeler, M. Kühne, S. Fecher, N. Gross, and J. Smet, Evidence of finite-momentum pairing in a centrosymmetric bilayer, Nat. Phys. **19**, 1599 (2023).

[20] X. Xi, H. Berger, L. Forró, J. Shan, and K. F. Mak, Gate tuning of electronic phase transitions in two-dimensional $NbSe_2$, Phys. Rev. Lett. **117**, 106801 (2016).

[21] K. Zhou, J. Deng, L. Guo, and J. Guo, Tunable superconductivity in 2*H*-$NbSe_2$ via *in situ* Li intercalation, Chin. Phys. Lett. **37**, 097402 (2020).

[22] J.-Y. Ji, T. Bao, H. Wang, Y. Xu, D. Zhang, and Q.-K. Xue, Homogeneous lateral lithium intercalation into transition metal dichalcogenides via ion backgating, Nano Lett. **22**, 7336 (2022).

[23] M. Liao, Y. Zhu, J. Zhang, R. Zhong, J. Schneeloch, G. Gu, K. Jiang, D. Zhang, X. Ma, and Q.-K. Xue, Superconductor-insulator transitions in exfoliated $Bi_2Sr_2CaCu_2O_{8+\delta}$ flakes, Nano Lett. **18**, 5660 (2018).

[24] A. Castellanos-Gomez, M. Buscema, R. Molenaar, V. Singh, L. Janssen, H. S. van der Zant, and G. A. Steele, Deterministic transfer of two-dimensional materials by all-dry viscoelastic stamping, 2D Mater. **1**, 011002 (2014).

[25] M. S. Whittingham and F. R. Gamble Jr., The lithium intercalates of the transition metal dichalcogenides, Mater. Res. Bull. **10**, 363 (1975).

[26] S. Fan, X. Zou, H. Du, L. Gan, C. Xu, W. Lv, Y.-B. He, Q.-H. Yang, F. Kang, and J. Li, Theoretical investigation of the intercalation chemistry of lithium/sodium ions in transition metal dichalcogenides, J. Phys. Chem. C **121**, 13599 (2017).

[27] Y. Nakagawa, Y. Kasahara, T. Nomoto, R. Arita, T. Nojima, and Y. Iwasa, Gate-controlled BCS-BEC crossover in a two-dimensional superconductor, Science **372**, 190 (2021).

[28] Y. H. Kim, S. Park, C. I. Kwon, S. Y. Kim, K. Watanabe, T. Taniguchi, and J. S. Kim, Two-dimensional multiband superconductivity of the optimally and uniformly Li-intercalated FeSe nanoflakes, Current Applied Physics **46**, 27 (2023).

[29] N. Werthamer, E. Helfand, and P. Hohenberg, Temperature and purity dependence of the superconducting critical field, H_{c2}. III. Electron spin and spin-orbit effects, Phys. Rev. **147**, 295 (1966).

[30] M. Calandra, I. I. Mazin, and F. Mauri, Effect of dimensionality on the charge-density wave in few-layer 2*H*-$NbSe_2$, Phys. Rev. B **80**, 241108(R) (2009).

[31] M. M. Ugeda, A. J. Bradley, Y. Zhang, S. Onishi, Y. Chen, W. Ruan, C. Ojeda-Aristizabal, H. Ryu, M. T. Edmonds, H.-Z. Tsai *et al.*, Characterization of collective ground states in single-layer $NbSe_2$, Nat. Phys. **12**, 92 (2016).

[32] A. Devarakonda, H. Inoue, S. Fang, C. Ozsoy-Keskinbora, T. Suzuki, M. Kriener, L. Fu, E. Kaxiras, D. C. Bell, and J. G. Checkelsky, Clean 2D superconductivity in a bulk van der Waals superlattice, Science **370**, 231 (2020).

[33] J. Qiao and D. Zhang, Extension of on-chip thermometry of metal strips toward sub-10 K regime, Appl. Phys. Lett. **120**, 173507 (2022).